Forest Science
https://doi.org/10.1007/s44391-025-00040-w

ORIGINAL ARTICLE

Comparing Juvenile Physiology and Morphology of Two High-Elevation Pines, *Pinus albicaulis* and *P. balfouriana*

Katherine Sparks[1] · Sean L. Hoy-Skubik[2] · Franklin Alongi[3] · Justin B. Runyon[4] · Katharine M. Banner[5] · Brian V. Smithers[2] · Danielle E. M. Ulrich[2]

Received: 9 April 2025 / Accepted: 15 July 2025

Abstract

Whitebark pine (*Pinus albicaulis*, PIAL) and foxtail pine (*P. balfouriana*, PIBA) are slow-growing, high-elevation, five-needled pines. Recently, PIAL has experienced significant mortality while PIBA has experienced minimal decline. PIBA exists in two disjunct southern ($PIBA_S$) and northern ($PIBA_N$) populations. Our study compared juvenile physiological and morphological traits between the two species (PIAL, PIBA) and foxtail populations ($PIBA_N$, $PIBA_S$) to investigate mechanisms underlying responses to environmental stressors in their high-elevation environments. We grew four-year-old PIAL and PIBA trees in a common greenhouse environment. We measured traits describing their morphology, biomass, stomatal and xylem conduit size and density, budburst phenology, gas exchange, whole plant volatile organic compounds (VOCs), phloem volatile resin (PVR) compounds, and non-structural carbohydrates (NSC). We found that PIAL and PIBA displayed different suites of traits that similarly promote resistance to environmental stressors (*e.g.,* high wind, drought, herbivores). The two PIBA populations did not differ in most traits except for VOCs where $PIBA_S$ emitted higher concentrations of specific and total whole plant VOCs than $PIBA_N$, suggesting that $PIBA_S$ may differ in susceptibility to stress from $PIBA_N$. For many traits and especially evident in whole plant VOC concentration and composition, PIAL and $PIBA_N$ were most similar while PIAL and $PIBA_S$ differed the most, consistent with growing season total precipitation of the juveniles' climates of origin. Our observed trait differences between species and populations offer insight into mechanisms by which PIAL and PIBA juveniles survive in their environments, improving our ability to understand drivers of current and future species distributions.

Keywords Seedling · Whitebark pine · Foxtail pine · Physiology · Volatile organic compounds · Treeline

Extended author information available on the last page of the article

Published online: 12 August 2025

Introduction

Whitebark pine (*Pinus albicaulis* Engelm.) and foxtail pine *(P. balfouriana* Balf.) are two of six North American high-elevation, five-needled pines ("high-five pines"), keystone and foundation species in subalpine ecosystems from southern California to Northern Canada (Gibson et al. 2008). High-five pines are slow-growing, pioneer species that often constitute the treeline of mountain ecosystems, characterized by high winds, unpredictable precipitation patterns, cold temperatures, snow, intense solar radiation, and nutrient-poor soils (Baumeister and Callaway 2006; Campbell et al. 2011). High-five pines provide habitat for other species, may stabilize snowpack, regulate downstream streamflow (Farnes 1990), and their seeds are often a main food source for wildlife including the grizzly bear (*Ursus horribilis* Linnaeus) and Clark's nutcracker (*Nucifraga columbiana* Wilson) (Felicetti et al. 2003; Schaming and Sutherland 2020). However, high-five pines, especially whitebark pine, have been experiencing high rates of mortality and decline due to a suite of abiotic and biotic stressors including increasing temperatures, drought, decreasing snowfall, non-native white pine blister rust (*Cronartium ribicola* J.C. Fisch), native mountain pine beetle (*Dendroctonus ponderasae* Hopkins), changing fire regimes, and competition with shade-tolerant conifers (Hansen et al. 2016; Tomback et al. 2022). High-five pines are particularly vulnerable to climate changes because the rate of temperature increase is high in mountain ecosystems, giving species less time to adapt (Pepin et al. 2015), and because subalpine species have less space to migrate to higher elevations as temperatures rise (Chang et al. 2014). Additionally, high-five pines have low growth rates, long generation times, delayed seed germination, and dispersal limitations, resulting in mortality outpacing regeneration (Tomback et al. 2001; Dullinger et al. 2004).

To better predict the distributions of high-five pines under future climates, we need to understand the physiological mechanisms, measured as traits, that underlie juvenile growth and survival under current and future climates. The ability of young developmental stages to survive into reproductively mature adults determines future species distributions (Hansen et al. 2021). However, high-five pine research focuses predominantly on adult tree mortality, with fewer studies investigating younger developmental stages that have different limiting stressors than adults. Physiological determinants of juvenile growth and survival include traits that affect the ability to obtain CO_2, water, and light, as well as traits that affect the ability to resist or tolerate abiotic and biotic stress. Examples of such physiological traits are photosynthetic performance, stomatal traits (*e.g.*, conductance, density, size), xylem characteristics (*e.g.*, tracheid density and size, potential hydraulic conductivity), non-structural carbohydrate (NSC) concentrations in needles, stems, and roots, and volatile organic compound (VOC) concentration and composition. For example, NSC (starch, sucrose, glucose, fructose) are products of photosynthesis that are used for essential functions including osmoregulation and as carbon reserves during stress-induced inhibited gas exchange (Hartmann and Trumbore 2016). NSC can also serve as substrate for the production of

VOCs, plant secondary compounds that are used in defense against biotic stressors (*e.g.,* fungal pathogens) as repellents or toxins, and abiotic stressors (*e.g.,* drought) through mechanisms like thermoregulation and cell stabilization (Rissanen et al. 2022). Examining physiological traits informs our understanding of how high-five pines physiologically respond to and persist in current and future environmental stress.

Currently, the high-five species of most concern in North America is whitebark pine (*P. albicaulis*; PIAL), which has experienced the highest rates of mortality (Goeking and Windmuller-Campione 2021). PIAL has the broadest and most northerly distribution of all high-five pines spreading latitudinally from California into northern Canada and the North American Rocky Mountains (Fig. 1). Across the western US, approximately 54% of whitebark pine trees were found to be dead during 2010–2019 (Goeking and Windmuller-Campione 2021). PIAL has been listed

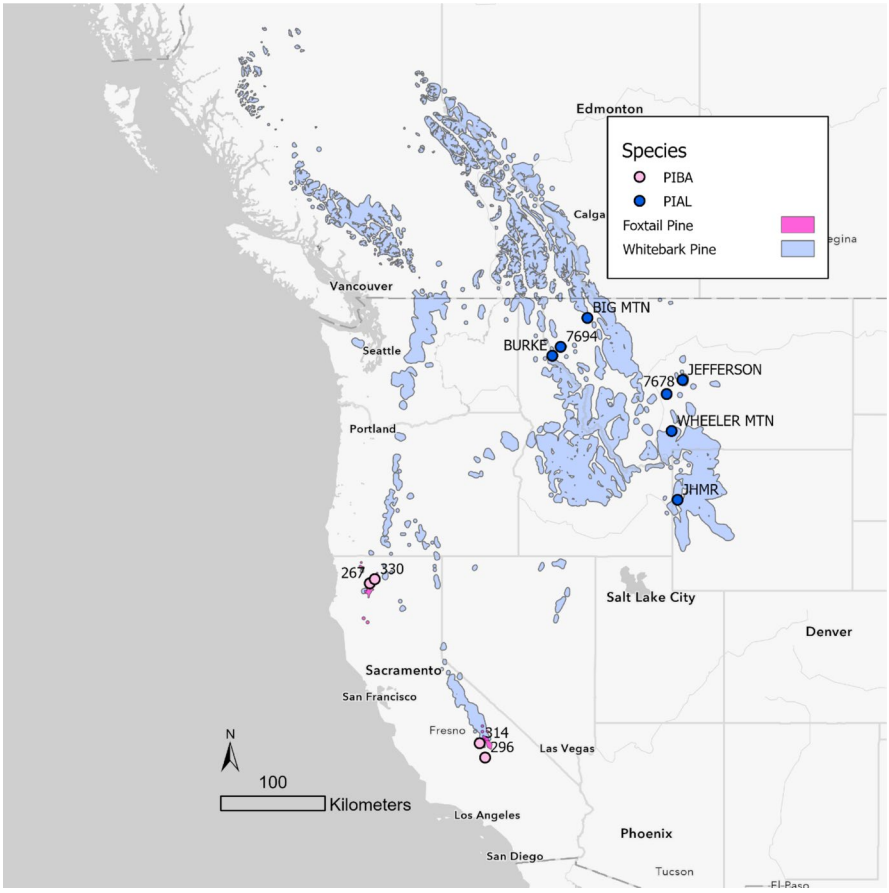

Fig. 1 Species distributions and family seed source names and locations (circles) for whitebark pine (PIAL, blue) and foxtail pine (PIBA, pink). $PIBA_N$ consists of families 267 and 330. $PIBA_S$ consists of families 314 and 296

as endangered under the Canadian Species at Risk Act since 2012 and was recently listed as threatened under the US Endangered Species Act in 2022 (Government of Canada 2017; USFWS 2022). While multiple stressors have played a role in the decline of PIAL, white pine blister rust, a non-native fungal pathogen, is the leading cause of mortality (Landguth et al. 2017). As a result, the primary restoration strategy is outplanting rust-resistant seedlings (Fiedler and McKinney 2014). However, the slow growth rate of PIAL leads to minimal recruitment and a decades-long delay between planting and stand regeneration (Tomback et al. 2001, 2022; Dullinger et al. 2004). Additionally, rust resistance is currently the only trait being selected for across PIAL seed sources, while tolerance to other stressors has been overlooked (Keane et al. 2017). This may limit restoration efforts if selected seedlings for outplanting cannot cope with multiple stressors (Schoettle et al. 2022).

In contrast to PIAL, foxtail pine (*P. balfouriana*; PIBA) is endemic within the US state of California (Fig. 1; Campbell et al. 2011) and is currently be listed as "near-threatened" by the International Union for Conservation of Nature (IUCN 2024), but has not received as much attention because PIBA has not declined nearly as much as PIAL. Across the western US, 17% of PIBA were found to be dead during 2010–2019 (Goeking and Windmuller-Campione 2021). PIBA has the lowest level of resistance to white pine blister rust of all high-five pines (Sniezko and Liu 2022), yet appears well-defended against mountain pine beetles due to high concentrations of phloem volatile resin and emission of VOCs that likely repel host-searching adults (Bentz et al. 2017; Nesmith et al. 2019; Schoettle et al. 2022). Though recent surveys show no white pine blister rust-induced declines in PIBA (Moore et al. 2017; Nesmith et al. 2019), rust infection has been documented in PIBA (Duriscoe and Duriscoe 2002). Increasing temperatures may expand the range and intensity of white pine blister rust infection within the PIBA distribution and reduce tree defense against the fungal pathogen and mountain pine beetles (Landguth et al. 2017; Wyka et al. 2018; Thoma et al. 2019; Young et al. 2023). For example, stress-induced reductions in photosynthesis may limit C available for VOC production and biotic defense. Additionally, sapling-sized recruitment of PIBA has declined, suggesting a bottleneck in recruitment from seedlings to saplings (Goeking and Windmuller-Campione 2021). Further research is needed to improve our understanding of the drivers of PIBA juvenile survival and mortality. Given that all high-five pines are susceptible to the same stressors (e.g., blister rust, bark beetle, changing climate) yet they exhibit differing levels of mortality to date (Goeking and Windmuller-Campione 2021), comparing PIBA, a species that has experienced some decline, with PIAL, a species that has experienced extensive decline, can help inform management strategies.

In contrast to the relatively unfragmented distribution of PIAL, PIBA has a uniquely disjunct distribution split between two geographically isolated populations. PIBA's distribution is divided by over 500 km into a southern population in the Sierra Nevada and a northern population in the Klamath mountains (Eckert et al. 2008). These two populations have been separated for 10,000–30,000 years so that the lack of gene flow between populations has created conditions for divergent evolution and potential speciation (Oline et al. 2000). For this reason, the species is split into two sub-species: *P. balfouriana* subsp. *balfouriana* (northern foxtail pine;

$PIBA_N$) and *P. balfouriana* subsp. *austrina* (southern foxtail pine; $PIBA_S$) (Bentz et al. 2017). Currently, little is known about how $PIBA_N$ and $PIBA_S$ may differ in their physiology and stress responses (Fryer 2004).

In our study, we investigated four research questions: are there juvenile physiological trait differences (1) between PIAL and PIBA?, (2) between $PIBA_N$ and $PIBA_S$?, (3) between PIAL and $PIBA_N$, and PIAL and $PIBA_S$?, and (4) How does drought stress affect the physiology of PIAL, $PIBA_N$, and $PIBA_S$ juveniles? Given that both species inhabit high-elevations with similar temperatures, we hypothesized that climate of origin, especially total precipitation, will influence differences in physiological traits for all comparisons. Specifically, we hypothesized that: (1) PIAL will exhibit drought resistant traits that allow PIAL to persist in a drier climate (with lower annual total precipitation) than PIBA, (2) $PIBA_S$ will exhibit drought resistant traits that allow $PIBA_S$ to persist in a drier climate than $PIBA_N$, (3) traits of PIAL will be more similar to those of $PIBA_S$ and most different from $PIBA_N$ because PIAL persists in a drier climate than PIBA and because $PIBA_S$ persists in a drier climate than $PIBA_N$, and (4) PIAL will resist drought stress more than $PIBA_N$ and $PIBA_S$. To test these hypotheses, we conducted a common environment greenhouse experiment exposing PIBA and PIAL juveniles to drought and control treatments and measured a suite of physiological and morphological traits before, during, and after drought treatment to compare the physiology, morphology, and stress responses between PIAL, $PIBA_N$, and $PIBA_S$.

Materials and Methods

Study Material

We obtained sixty-two four-year-old (juvenile) whitebark pine individuals (*Pinus albicaulis,* PIAL) from the Coeur d'Alene USDA Forest Service Nursery (Coeur d'Alene, ID, USA), and nineteen four-year-old foxtail pine individuals (*Pinus balfouriana,* PIBA) from the Dorena Genetic Resource Center USDA Forest Service Nursery (Cottage Grove, OR, USA). PIAL juveniles were grown from seed collected from seven parent trees (families) in Idaho (Burke), Montana (Big Mountain, Jefferson, Wheeler Mountain, '7694', '7678'), and Wyoming (JHMR) (Fig. 1, Table S1). PIBA juveniles were grown from seed collected from two populations: the northern population ($PIBA_N$) and the southern population ($PIBA_S$), each composed of two families (Fig. 1, Table S1). Average annual, growing season (June–September), and winter (May–October) climate variables (based on 30-year-normal monthly values) of each species and population were obtained from PRISM Climate Group at Oregon State University (n.d.) (Table 1). Growing season was determined based on the months with average temperatures above 7ºC (Tran et al. 2017; Bunn et al. 2018).

PIAL and PIBA juveniles were transplanted into tree pots (19 cm × 19 cm × 46 cm) with a peat-perlite soil medium (Sunshine #1 mix – Sungro, Agawam, MA, USA) on 17 January 2022 and 8 April 2022, respectively, and placed in the Plant Growth Center (Montana State University). Plants were watered to maintain 25% soil volumetric water content (VWC), measured weekly (Hydrosense II, Campbell

Table 1 Whitebark pine (PIAL) and foxtail pine (PIBA) seed source location (Fig. 1) and climate (precipitation (mm), temperature (°C), VPD (vapor pressure deficit, hPa)) from 1991–2020 (Prism Climate Group, 2020; 800 m resolution) for annual, growing season (June–September), and winter (October-May) timeframes averaged across families. Locations of each family are listed in Table S1

		PIAL	PIBA	North PIBA ($PIBA_N$)	South PIBA ($PIBA_S$)
	Latitude (°)	46.6	38.8	41.3	36.2
	Longitude (°)	−112.8	−120.6	−122.7	−118.4
	Elevation (m)	2203.7	2580.3	2250.0	2910.5
Annual	Mean Precipitation	95.9	120.4	156.8	83.9
	Total Precipitation	1151.7	1444.2	1881.1	1007.2
	Average Minimum Temperature	−2.3	−0.1	1.4	−1.5
	Average Temperature	2.7	5.3	6.1	4.4
	Average Maximum Temperature	7.7	10.7	10.9	10.4
	Average Dewpoint	−3.7	−4.3	−2.7	−5.9
	Average Minimum VPD	1.5	2.7	2.8	2.6
	Average Maximum VPD	7.1	10.0	9.6	10.4
	Average VPD	4.3	6.4	6.2	6.5
Growing Season (June–September)	Mean Precipitation	59.9	21.1	29.7	12.5
	Total Precipitation	239.6	84.5	118.8	50.2
	Average Minimum Temperature	5.9	6.9	8.0	5.7
	Average Temperature	12.2	12.8	13.8	11.8
	Average Maximum Temperature	18.6	18.7	19.6	17.8
	Average Dewpoint	2.5	0.9	1.8	0.1
	Average Minimum VPD	3.1	4.8	5.2	4.4
	Average Maximum VPD	13.8	16.4	16.9	16.0
	Average VPD	8.5	10.6	11.0	10.2
Winter Season (October-May)	Mean Precipitation	114.0	170.0	220.3	119.6
	Total Precipitation	912.1	1359.7	1762.3	957.1
	Average Minimum Temperature	−6.3	−3.5	−2.0	−5.1
	Average Temperature	−2.0	1.5	2.3	0.8
	Average Maximum Temperature	2.3	6.6	6.6	6.7
	Average Dewpoint	−6.8	−6.9	−4.9	−8.9
	Average Minimum VPD	0.8	1.6	1.6	1.7
	Average Maximum VPD	3.8	6.8	6.0	7.6
	Average VPD	2.3	4.2	3.8	4.6

Scientific, Logan, UT, USA) and hourly (GroPoint Lite, Riot Technology Corp., North Saanich, BC, Canada; CR-1000X data logger, Campbell Scientific, Logan, UT, USA). Supplemental lighting maintained a minimum 16-h photoperiod. In the greenhouse, daytime photosynthetically active photon flux density averaged 843 μmol m^2 s^{-1}, temperatures averaged 20.7°C during the day and 16.4°C during the night, and average relative humidity was 56%.

Treatments began on 12 June 2022 and ended on 9 December 2022, lasting 24 weeks. In the drought treatment, we reduced the target VWC to 5% based on previous measurements to create moderate drought conditions using a method adapted from Marchin et al. (2020). Tree pots were firmly placed atop floral foam blocks (Smithers-Oasis, Kent, OH, USA) that sat in large, plastic bins (102 L) that each held six pots. Each pot had nine 2-cm diameter holes drilled in the bottom of each pot to provide connection between soil and floral foam. We controlled VWC for the drought and control treatments by varying the water level within each bin, which was determined in a pilot study using 12 PIAL juveniles not included in this study. The water level was set at 20 cm for control bins and 10 cm for drought bins during the first ten weeks of the experiment, and then set to 10 cm for control bins and 0 cm for drought bins during the remainder of the experiment to reach the VWC target of 5%.

Treatment (drought, control) was randomly assigned to each bin. Then, juveniles were randomly distributed to each bin ($n = 4$–6) using an unbalanced incomplete block design to account for unequal sample sizes between species with each family and species represented as equally as possible in each bin. VWC was measured weekly and hourly with sensors placed directly in the soil for one juvenile per bin and divided so PIAL, $PIBA_N$, and $PIBA_S$ had at least one sensor in both drought and control treatments. Morphological and stomatal traits were measured prior to treatment. Physiology, volatile organic compounds, and budburst phenology were measured throughout the experiment. Following the experiment, we harvested all juveniles for biomass, xylem, and NSC measurements. Individuals were measured, sampled, and harvested in a stratified randomized order designed to equally distribute species and families across multiple consecutive days if needed.

Morphology

Morphological trait measurements were made 10–25 March 2022. We measured stem base diameter (cm), stem height (cm), stem base diameter to stem height ratio (stem diameter:stem height), fascicle density (FD, number of fascicles per branch length), branch diameter (mm), branch length (mm), branch diameter to branch length ratio (branch diameter:branch length), leaf mass per area (LMA; g mm^{-1}), sapwood area to leaf area ratio (A_S:A_L), and the ratio of sunlit canopy leaf area to total leaf area (STAR). For branch diameter, branch length, branch diameter:branch length, and FD, we selected three first order lateral branches and measured their diameter one centimeter from the main stem and their length from main stem to apical bud and counted the total number of fascicles on the branch. FD was calculated for each of the three branches as the total number of fascicles divided by total branch length. FD, branch diameter, branch length, and branch diameter:branch length were averaged across the three branches for each individual. LMA was calculated for the largest first order lateral branch as the ratio of dry leaf mass to fresh leaf area. Fresh leaf area was measured using Fiji (previously ImageJ; Schindelin et al. 2012). We measured dry leaf mass after drying for 72 h at 45 °C. A_S:A_L was calculated as the ratio of sapwood area (defined as functional conducting tissue) to fresh leaf area.

Sapwood area (A_S) was determined by cutting a 0.25-cm section from the base of the branch (same branch used to measure fresh leaf area) to expose the cross section. We imaged the cross section and analyzed images in Fiji measuring the cross-sectional area minus the bark area. STAR was calculated as the ratio of the total sun-exposed canopy leaf area to the total fresh leaf area for the whole individual. To measure total sun-exposed leaf area, we used Trainable WEKA Segmentation (TWS), a plug-in available for Fiji, on top-down images of each individual on a neutral background. We trained the TWS default classifier, FastRandomForest (Reutemann 2022), on 20 images (ten from each species) to identify the individual from the neutral background. We ran all images through our trained classifier using the Fiji macros plug-in. The classifier created probability maps which we converted to binary 8-bit images prior to measuring leaf area. Total fresh leaf area was calculated using the following equation:

$$A_T = m_T \bullet \frac{A_b}{m_b}, \tag{1}$$

where A_T is total fresh leaf area, m_T is total dry leaf mass, A_b is the previously measured fresh leaf area from the largest first order lateral branch (from LMA), and m_b is the previously measured dry leaf biomass from the largest first order lateral branch (from LMA).

Stomatal Traits

Stomatal traits included aperture area (μm^2), guard cell area (μm^2), stomatal length (mm), and stomatal density (number stomata mm^{-1}) and were measured between 9–23 March 2022. Five needles were taken from each of the three branches previously selected for FD measurements (described above). Fresh needles were stored in sealed plastic bags with moist paper towels in the dark between sampling and processing, which occurred within five hours of collection. Fresh stomatal impressions were made using clear nail polish across the abaxial side of the needle and clear cellophane tape to affix the impression onto a slide to view under a light microscope (Micromaster, Fisher Scientific, Hampton, NH, USA) at 100 × magnification. The highest quality portion of the impression was imaged (Swift Imaging 3.0 software with a SwiftCam SC500, Swift Optical Instruments, Shertz, TX, USA), and guard cell area was measured (Fiji) by circling the entire stomate (aperture area and guard cell area) and subtracting aperture area from the total stomatal area. Stomatal density was measured as the number of stomata per row divided by row length.

Physiological Traits

During 15 June-28 November 2022, leaf gas exchange, predawn and midday leaf water potentials ($\Psi_{pd,}$ Ψ_{md}, MPa) and leaf temperature (°C) were measured weekly on each juvenile. Leaf-area-corrected net photosynthetic rate (A_{net}, mmol CO_2 m^{-2} leaf area s^{-1}) and stomatal conductance (g_s, mmol H_2O m^{-2} leaf area s^{-1}) were measured using a portable infrared gas analyzer (LI-6800, LI-COR, Lincoln, NE

USA) with the cuvette environment set to the following: 1000 µmol m^{-2} s^{-1} photosynthetic photon flux density, 60% relative humidity, 400 ppm [CO_2], 25 °C leaf temperature, and 500 µmol s^{-1} flow rate. Leaf temperature was measured using an infrared thermometer held ten centimeters from the same cluster of needles selected for gas exchange measurements. Ψ_{pd} and Ψ_{md} were measured using a pressure chamber (PMS Instrument Company, Albany, OR, USA) on two needles each collected at two timepoints: one hour before dawn (3h00-6h00) and at 12h30, respectively. A visual health score for each individual was determined on a scale of 0–5 based on both the coloring (i.e., vivid green, muted green, yellowing, yellow, browning, or dead) with zero being dead and five being healthy.

Volatile Organic Compounds (VOCs)

Whole plant volatile organic compounds (VOCs) were measured at three timepoints (11 June, 8 August, 28 November 2022; $N = 9$–40) using the headspace method (Burkle and Runyon 2017). To measure whole plant VOC emission for each juvenile, we secured a Teflon bag (50 cm wide × 75 cm deep, American Durafilm Co., Holliston, MA, USA) around the entire aboveground tissue of each juvenile, which contained a 30-mg absorbent volatile trap (HayeSep-Q, Restek, Bellefonte, PA, USA). Air was pumped out of the bag through the volatile trap using a vacuum pump for 45 min per juvenile at 0.5 L/min. Traps were kept on ice and transported to the USDA Forest Service, Rocky Mountain Research Station (USDA FS RMRS) lab in Bozeman, MT, USA, sealed and stored at 4 °C, and processed within three weeks of collection. We eluted traps with 200 µL of dichloromethane and a gentle stream of ultra-high-purity nitrogen gas was used to push out the remainder of the solvent; 1 µg of *n*-nonyl acetate was added as the internal standard. Aboveground biomass of dried stems and needles was used to calculate whole plant VOCs as ng of compound per gram of aboveground biomass per hour (ng g^{-1} biomass h^{-1}).

Phloem volatile resin (PVR) samples were collected in December 2022 ($N = 8$–23) following Runyon et al. (2022). A 0.5-cm-long section of fresh stem was immediately placed on ice and transported to the USFS RMRS lab, where samples were stored at −80°C. For sample analysis, we removed all the outer bark from each frozen sample prior to removing the phloem. Approximately 25 mg of frozen phloem was cut into small pieces (~2 mm^3), placed in 1 mL of 95% *n*-Hexane (Sigma-Aldrich, St. Louis, MO; ACS reagent grade), and agitated at room temperature for 24 h. Solvent was then transferred to new vials and an additional 0.25 mL of hexane was used to rinse the remaining phloem pieces twice, resulting in a final volume of 1.5 mL in the new vials. 100 µg of *n*-nonyl acetate was added as the internal standard. The remaining phloem pieces were placed in a drying oven for one week and weighed. Compound concentrations were analyzed on a dry phloem weight basis (mg of compound per gram of phloem; mg g^{-1}).

Both processed samples from VOCs and PVR were analyzed using a gas chromatograph-mass spectrometer (GC–MS, Agilent 7890 A GC coupled with a 5975 C MS) and separated on a nonpolar capillary column (HP-1ms, 30 m × 0.25 mm i.d, 0.25 µm film thickness) column with helium carrier gas. One mL of each sample

was injected using splitless mode (injector 225 °C) with the GC oven maintained at 60 °C for 10 min, then increased 2.5 °C min^{-1} to 160 °C, then 30 °C min^{-1} to 225 °C. Quantifications were made relative to the internal standard (ChemStation software, Agilent Technologies, Wilmington, DE, USA). We used the NIST 08 Mass Spectral Search Program (National Institute of Standards and Technology, Gaithersburg, MD, USA) to identify compounds and confirmed them using commercial standards, when available.

Budburst Phenology

Budburst monitoring occurred 1 March-28 November 2022. We visually assigned the terminal buds of each juvenile to one of six budburst stages once a week, with stage one being a closed bud and stage six being needle elongation (Martínez-Berdeja et al. 2019; Ulrich et al. 2023). We calculated the number of days from stage one to each budburst stage.

Biomass

After the experiment ended, biomass measurements (needle, stem, root, aboveground:belowground; g) were made in December 2022. We harvested each juvenile from the pot, removed soil, and separated, dried, and weighed needles, stems, and roots.

Xylem Traits

A 1-cm fresh stem segment was cut from the base of each harvested juvenile stem, dried for 72 h at 45 °C before being rehydrated and embedded in paraffin wax to stabilize cell structure for sectioning. Stem samples were sectioned transversely using a hand sliding rotary microtome (Leica Biosystems, Wetzlar, Germany) set at 16-µm thickness. Sections were fixed to slides and deparaffinized, then stained with toluidine blue for clear visualization. We imaged stained sections with a standard light microscope (Micromaster, Fisher Scientific, Hampton, NH, USA) at 100× and 1000× magnification using a microscope camera (Swiftcam SC1003-CK, Swift Optical Instruments, Shertz, TX, USA) and Swift Imaging 3.0 software. We stitched together image tiles (100× magnification) to create a complete stem cross section (Fiji).

We measured annual earlywood (EW) ring width, annual latewood (LW) ring width, annual total ring width, resin duct area and density, EW and LW tracheid area, EW and LW tracheid density, EW and LW cell wall thickness, potential hydraulic conductivity (K_p), and vessel implosion resistance (VIR, a proxy for structural integrity). We measured EW ring width and LW ring width at four haphazardly selected locations per growth ring and averaged them to obtain a single EW, LW, and annual (EW + LW) width per ring per individual. For resin duct area, we measured the area of all resin ducts within a stem cross section and calculated mean resin duct area. Resin duct density was calculated as the total number of resin ducts divided

by total mm^2 of the stem cross section. For EW and LW tracheid area and cell wall thickness, we measured all cells in three randomly selected EW and LW 9.97×10^{-3} mm^2 sections per growth ring at 1000 × magnification for a total of six measured sections per growth ring. To measure tracheid area, we circled all tracheids in each imaged section for all six 1000 × sections (freehand tool in Fiji). To measure tracheid cell wall thickness, we measured 25 total double cell walls per imaged section and divided each double cell wall thickness by two to achieve 50 total single cell wall measurements per imaged section (line tool in Fiji).

Potential hydraulic conductivity (K_p) was calculated using the Hagen-Poiseuille equation for EW and LW separately (K_{pEW}, $_{KpLW}$). We calculated K_p as (Sterck et al. 2008):

$$K_p = K_{pEW} + K_{pLW}, \tag{2}$$

where K_{pEW} and K_{pLW} were calculated as (Yang et al. 2022):

$$K_{pEW} = \frac{\pi \rho_w}{128\eta} \times CD_{EW} \times D_{EW}^4, \tag{3}$$

$$K_{pLW} = \frac{\pi \rho_w}{128\eta} \times CD_{LW} \times D_{LW}^4, \tag{4}$$

And where ρ_w is the density of water (998.2 kg m^{-3} at 20 °C), η is the viscosity of water (1.002×10^{-3} Pa • s at 20 °C), CD is the mean conduit density, and D (vessel diameter) is calculated separately for LW and EW using the following equation (Steppe and Lemeur 2007):

$$D = \sqrt[4]{\frac{1}{n} \sum_{i=1}^{n} \frac{2a_i^3 b_i^3}{a_i^2 + b_i^2}}, \tag{5}$$

where n is the number of conduits measured, and a and b are the major and minor axes (respectively) of the assumed "ellipse" created by the lumen area. Vessel implosion resistance (VIR) was calculated as:

$$\text{VIR} = (t/b)_h^2, \tag{6}$$

where t is the double wall thickness and b is the conduit wall span. Double wall thickness was measured directly from 1000 × magnification images. Conduit wall span was estimated as one side of a square with an area equal to mean conduit area (Hacke et al. 2001).

Non-Structural Carbohydrates (NSC)

Following the destructive harvest, separated roots, stems, and needles (except for the sample of stem used for xylem and phloem analyses) were microwaved for three minutes in one-minute intervals to halt enzymatic activity (Landhäusser et al. 2018). The separated plant tissue was dried for 72 h at 45 °C, weighed for biomass (described

above), and then ground to a fine powder. The concentration of total non-structural carbohydrates (NSC), glucose, sucrose, fructose, and starch (mg compound g^{-1} dry weight plant material) were measured separately for roots, stems, and needles of each individual following the enzyme method (Landhäusser et al. 2018; Ulrich et al. 2023).

Statistical Analysis

All analyses were conducted in R (R Core Team, 2023). We used each trait as a response variable in a separate linear mixed effects (LME) model with treatment (drought, control) and species (PIAL, PIBA) as fixed effects and bin and family as random effects. We used post hoc linear contrasts (*lme4 v*1.1.34*, emmeans* v1.8.8) to estimate marginal mean differences for the following comparisons: PIAL *vs.* PIBA, PIAL *vs.* $PIBA_N$, PIAL *vs.* $PIBA_S$, and $PIBA_N$ *vs.* $PIBA_S$. In order to identify how specific individual traits differed in our comparisons of interest, we assumed that each response variable was completely independent though they were measured on the same individual. We accounted for conducting four difference in mean comparisons for each trait with the *mvt* multivariate adjustment. For physiological traits (A_{net}, g_s, $\Psi_{pd,}$ Ψ_{md}, Ψ_{md}-Ψ_{pd}, T_{leaf}), we used the above-described model, but with date as an additional fixed effect and tree ID as an additional random effect (as there were weekly repeated measures for these traits). Normality and linearity assumptions were checked with residual plots for all LME models. Sample sizes for all measurements are in Table S2 and S3.

We visualized compositional differences between groups (PIAL, $PIBA_N$, $PIBA_S$) for all whole plant VOC and PVR compounds with non-metric multidimensional scaling (NMDS) plots using Bray–Curtis dissimilarity matrices (*vegan* v6.1). We used random forest analysis to identify specific influential compounds. We used five random forest models with all identified compounds as predictors and one of the following as a response variable for each model: 1) PIAL *vs.* PIBA, 2) PIAL *vs.* $PIBA_N$, 3) PIAL *vs.* $PIBA_S$, and 4) $PIBA_N$ *vs.* $PIBA_S$. We then calculated mean decrease accuracy as the loss of accuracy with that compound removed from the model. To examine differences in concentrations of some of the most influential compounds identified with data from our study, we selected the top four most influential whole plant VOC and PVR compounds from each comparison. To estimate mean marginal differences in concentrations of these influential compounds for each comparison, we used LME models and post hoc linear contrasts (*lme4 v*1.1.34*, emmeans* v1.8.8) with treatment and species as fixed effects and bin and family as random effects. For whole plant VOCs collected at three different timepoints, we also included date and tree ID as random effects.

Results

PIAL vs. PIBA

Climate of origin of PIAL was drier than that of PIBA annually (total precipitation of PIAL = 1152 mm, PIBA = 1444 mm) and especially during the winter season (total precipitation of PIAL = 912 mm, PIBA = 1360 mm) (Table 1, Figure S1).

In the growing season however, PIBA climate was drier than that of PIAL (total precipitation of PIBA = 85 mm, PIAL = 240 mm). This resulted in 94% of PIBA annual precipitation and 79% of PIAL annual precipitation falling during the winter. For morphology traits, in comparison to PIAL, PIBA exhibited smaller stem and branch diameters, lower branch diameter:branch length, taller stems, and lower stem diameter:stem height (Fig. 2A, Table S2). PIAL had higher LMA (leaf mass per area, Fig. 2B) and total canopy area (leaf + woody tissue) than PIBA, while PIBA had lower STAR (sunlit leaf area to total leaf area ratio) than PIAL. Biomass traits did not differ between species. For stomatal traits, PIBA had larger stomatal (aperture) area (Fig. 2C), aperture length, and guard cell area than PIAL, but stomatal density and total number of stomata did not differ between species. For xylem traits, PIBA had higher LW tracheid density (Fig. 2D) and EW cell wall thickness than PIAL, and smaller LW lumen area (Fig. 2E) and lower K_p (potential conductivity, Fig. 2F) than PIAL. Also, PIBA had higher mean resin duct density (Fig. 3A) and mean resin duct area than PIAL. For budburst phenology traits, PIAL reached stages 2, 3, and 6 earlier than PIBA. We found no evidence of a difference in means between species for any of the measured physiological traits from LME models.

A total of 41 whole plant VOCs and 55 PVR (phloem volatile resin) compounds were identified from both PIAL and PIBA. The blend of VOCs emitted by PIAL and PIBA was qualitatively the same. Random forest analysis identified the most influential whole plant VOCs and PVR compounds driving the separation between species (Table 2). Of the influential whole plant VOCs, PIBA had higher concentrations of β-pinene (Fig. 3B) and lower concentrations of unknown sesquiterpene 5 than PIAL, but unknown benzene 1 or limonene concentrations did not differ between species. Of the influential PVR compounds, PIBA had higher concentrations of α-pinene (Fig. 3C), and lower concentrations of limonene and unknown sesquiterpenes 21 and 22. However, total whole plant VOC (Fig. 4A) and PVR compound (Fig. 5A) concentrations did not differ between species. In the NMDS plot of all whole plant VOCs, we observed overlap in compounds of PIAL, $PIBA_N$, and $PIBA_S$, creating a transitional gradient from PIAL to $PIBA_N$ to $PIBA_S$, with $PIBA_N$ overlapping with the two groups, and more separation between PIAL and $PIBA_S$ (Fig. 4B). In contrast, for all PVR compounds, we observed clear separation between PIAL and PIBA where $PIBA_N$ and $PIBA_S$ grouped together (Fig. 5B).

For NSC, PIBA had higher concentrations of needle and stem glucose, needle sucrose, needle and stem soluble sugars (glucose + fructose + sucrose) (Fig. 3D), stem combined glucose + fructose, and stem total NSC (glucose + fructose + sucrose + starch) than PIAL. We found no evidence of a difference between species in means of NSC concentrations in roots and starch concentrations in all tissue types from LME models.

$PIBA_N$ vs. $PIBA_S$

Climate of origin of $PIBA_S$ was drier than that of $PIBA_N$ annually (total precipitation of $PIBA_S$ = 1007 mm, $PIBA_N$ = 1881 mm) and during the growing season (total

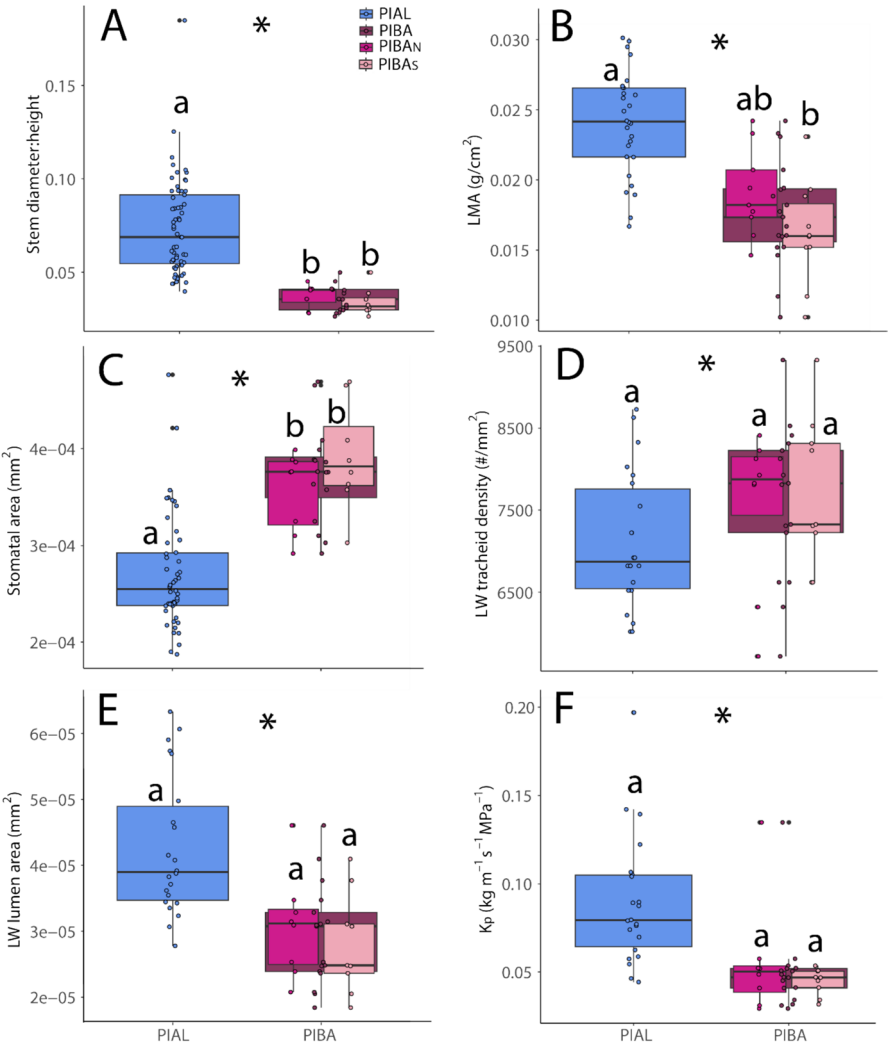

Fig. 2 Boxplots of key traits of PIAL, PIBA, $PIBA_N$, and $PIBA_S$. Top and bottom lines represent first and fourth quartiles and boxes represent the second and third quartiles split by the median line. Asterisks represent significant differences between species ($p \leq 0.05$). Lowercase letters represent significant differences between PIAL, $PIBA_N$, and $PIBA_S$ ($p \leq 0.05$). **A** is the ratio of stem diameter to stem height (stem diameter:height, $N = 8$–62), **B** is leaf mass per area (LMA, $N = 9$–28), **C** is stomatal aperture area (stomatal area, $N = 8$–50), **D** is latewood (LW) tracheid density ($N = 8$–23), **E** is latewood (LW) lumen area ($N = 8$–23), and **F** is potential hydraulic conductivity (K_p, $N = 8$–23) (Table S2)

precipitation of $PIBA_S = 50$ mm, $PIBA_N = 119$ mm) and winter season (total precipitation of $PIBA_S = 957$ mm, $PIBA_N = 1762$ mm) (Table 1, Figure S1).

We observed evidence for PIBA population differences in means of only two non-VOC traits and five VOC traits based on LME models (Table S2). Compared to $PIBA_N$, $PIBA_S$ had higher A_S:A_L, lower EW cell wall thickness, and higher

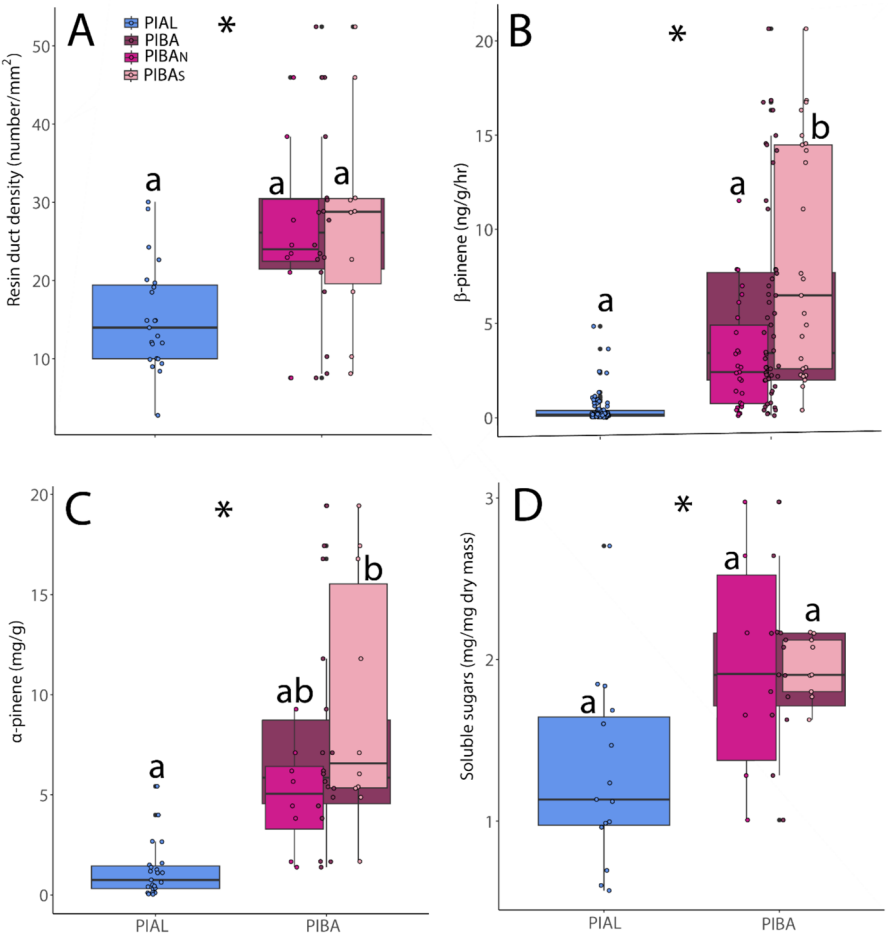

Fig. 3 Boxplots of key traits of PIAL, PIBA, $PIBA_N$, and $PIBA_S$. Top and bottom lines represent first and fourth quartiles and boxes represent the second and third quartiles split by the median line. Asterisks represent significant differences between species ($p \leq 0.05$). Lowercase letters represent significant differences between PIAL, $PIBA_N$, and $PIBA_S$ ($p \leq 0.05$). **A** is mean resin duct density ($N = 8$–23), **B** is VOC β-pinene concentration from whole plant ($N = 9$–40), **C** is α-pinene concentrations from phloem volatile resin (PVR, $N = 8$–23), and **D** is the concentration of needle soluble sugars (glucose, fructose, sucrose; mg compound/g dry weight plant material, $N = 6$–15) (Table S2)

concentrations of specific whole plant VOCs (β-pinene (Fig. 3B), unknown benzene 1, unknown monoterpene 4), concentrations of total whole plant VOCs (Fig. 4A), and one PVR compound methyl thymyl ether. The most influential whole plant VOCs driving the separation between $PIBA_N$ to $PIBA_S$ were: β-pinene (higher in $PIBA_S$ than $PIBA_N$), unknown sesquiterpene 5, unknown monoterpene 1, and 3-carene (Table 2). None of the influential PVR compound concentrations driving the separation between $PIBA_N$ to $PIBA_S$ did not significantly differ between

Table 2 The top four influential compounds for each comparison (PIAL vs PIBA, PIAL vs $PIBA_N$, PIAL vs $PIBA_S$, $PIBA_N$ vs $PIBA_S$). Bolded compounds significantly differed ($p \leq 0.05$)

	PIAL vs PIBA	PIAL vs $PIBA_N$	PIAL vs $PIBA_S$	$PIBA_N$ vs $PIBA_S$
Whole Plant Volatile Organic Compounds (VOCs)	**β-Pinene**	β-Pinene	**β-Pinene**	**β-Pinene**
	Unknown Benzene 1	Unknown Benzene 1	**Unknown Benzene 1**	
	D-limonene			
	Unknown Sesquiterpene 5	Unknown Sesquiterpene 5		Unknown Sesquiterpene 5
		Unknown Sesquiterpene 7		
			Unknown Monoterpene 1	Unknown Monoterpene 1
			3-Carene	3-Carene
Phloem Volatile Resin (PVR) compounds	**α-Pinene**	α-Pinene		α-Pinene
	Limonene	Limonene		Limonene
		Unknown Sesquiterpene 4		
	Unknown Sesquiterpene 21			
	Unknown Sesquiterpene 22	Unknown Sesquiterpene 22		
			Terpinolene	Terpinolene
			γ-Terpinene	
			Methyl-thymyl-ether	
			Sabinene	Sabinene

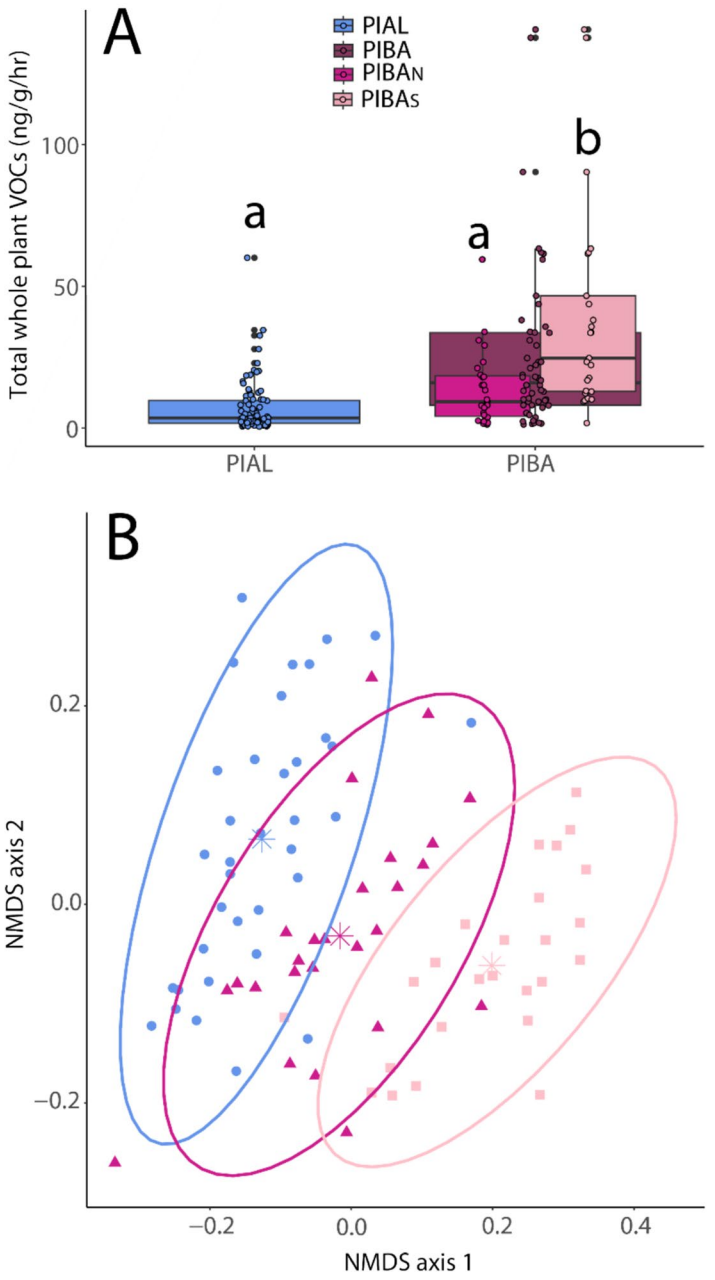

Fig. 4 **A** Boxplots of total whole plant VOC concentrations (ng/g/hr) for PIAL, PIBA, $PIBA_N$, and $PIBA_S$ ($N = 9$–40). Top and bottom lines represent first and fourth quartiles and boxes represent the second and third quartiles split by the median line. Lack of asterisk indicates no significant difference between species ($p \leq 0.05$). Lowercase letters represent significant differences between PIAL, $PIBA_N$, and $PIBA_S$ ($p \leq 0.05$). **B** Nonmetric multidimensional scaling (NMDS) plot of whole plant VOCs of PIAL, $PIBA_N$, and $PIBA_S$ ($N = 9$–40). Central stars are the centroids for each group calculated as the average across the x- and y-axes for each group. Ellipses represent bivariate confidence intervals assuming t-distribution

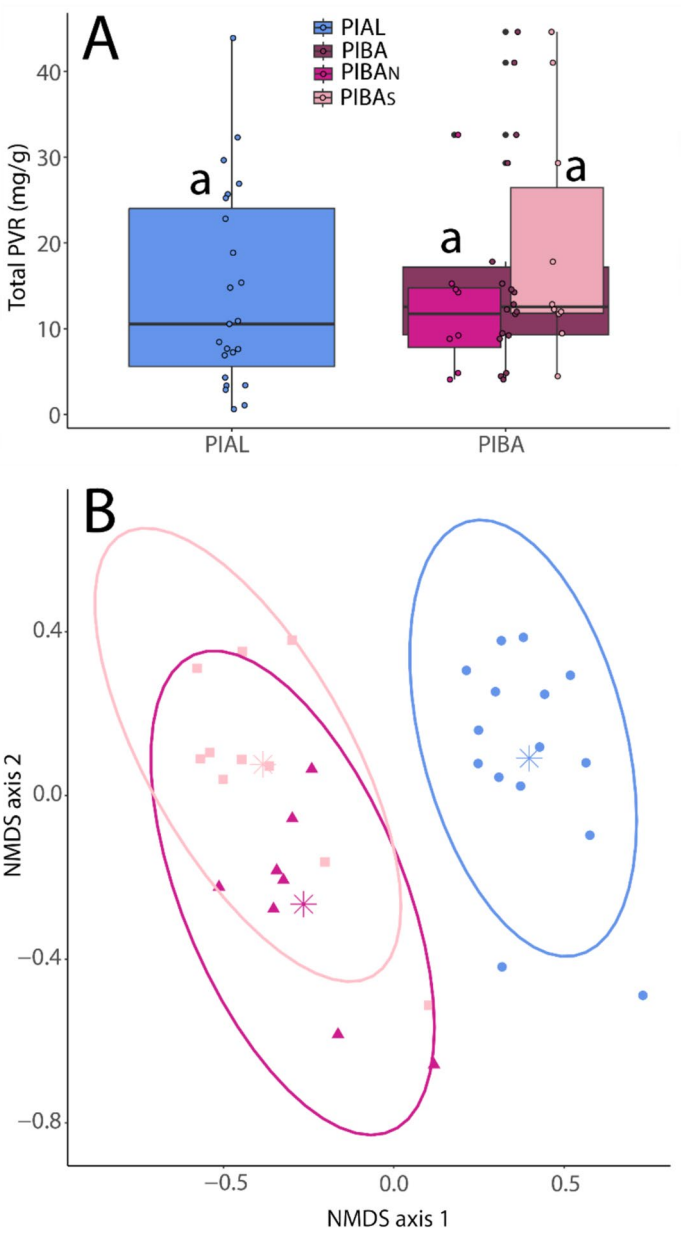

Fig. 5 **A** Boxplots of total PVR concentrations (mg/g) for PIAL, PIBA, $PIBA_N$, and $PIBA_S$ ($N = 8–23$). Top and bottom lines represent first and fourth quartiles and boxes represent the second and third quartiles split by the median line. Lack of asterisk indicates no significant difference between species ($p \leq 0.05$). Lowercase letters represent significant differences between PIAL, $PIBA_N$, and $PIBA_S$ ($p \leq 0.05$). **B** Nonmetric multidimensional scaling (NMDS) plot of phloem volatile resin (PVR) compounds of PIAL, $PIBA_N$, and $PIBA_S$ ($N = 8–23$). Central stars are the centroids for each group calculated as the average across the x- and y-axes for each group. Ellipses represent bivariate confidence intervals assuming t-distribution

populations (Tables 2, S2). The NMDS plot showed overlap between populations for whole plant VOCs (Fig. 4B) and PVR compounds (Fig. 5B). We found no evidence of a species difference in means of any NSC concentration in any tissue type from LME models.

PIAL vs.$PIBA_N$ and PIAL vs.$PIBA_S$

$PIBA_S$ annual total precipitation was the lowest of the three groups, followed by PIAL and then $PIBA_N$ (annual total precipitation of $PIBA_S = 1007$ mm, PIAL = 1152 mm, $PIBA_N = 1881$ mm) (Table 1, Figure S1). $PIBA_S$ growing season total precipitation was also the lowest of the three groups, but followed by $PIBA_N$ and then PIAL (total precipitation of $PIBA_S = 50$ mm, $PIBA_N = 119$ mm, PIAL = 240 mm). In contrast, PIAL winter season precipitation was lowest of the three, followed by $PIBA_S$ and then $PIBA_N$ (total precipitation of PIAL = 912 mm, $PIBA_S = 957$ mm, $PIBA_N = 1762$ mm). This resulted in 79% of PIAL annual precipitation falling during winter compared to 94% of $PIBA_N$ and 95% of $PIBA_S$ precipitation falling in winter.

$PIBA_N$ differed from PIAL in 13 traits while $PIBA_S$ differed from PIAL in 16 traits based on LME models (Table S2). In three of those traits, both PIBA populations differed from PIAL where both $PIBA_N$ and $PIBA_S$ had lower stem diameter:stem height (Fig. 2A) and canopy leaf area, and higher stomatal area (Fig. 2C) than PIAL. Compared to PIAL, $PIBA_N$ had lower stem diameter:stem height (Fig. 2A) and canopy leaf area, higher stomatal area (Fig. 2C), stomatal aperture length, and number of rows of stomata, lower resin duct area, higher earlywood cell wall thickness, more days to reach budburst stage 2, higher unknown sesquiterpene 4 (PVR), and higher stem glucose, glucose + fructose, total NSC, and sugars (glucose, fructose, sucrose). Compared to PIAL, $PIBA_S$ had smaller stem diameter, greater stem height, lower stem diameter:stem height (Fig. 2A), lower LMA (Fig. 2B), higher A_S:A_L, lower STAR and canopy leaf area, larger stomatal and guard cell area, higher concentrations of specific whole plant VOCs (β-pinene (Fig. 3B), unknown benzene 1, unknown monoterpenes 3 and 4), higher total whole plant VOCs (Fig. 4A), and higher concentrations of specific PVR compounds (α-pinene (Fig. 3C), methyl thymyl ether).

Random forest analysis revealed that the most influential whole plant VOCs driving the separation between both $PIBA_N$ and PIAL, and $PIBA_S$ and PIAL were β-pinene and unknown benzene 1, with $PIBA_S$ (but not $PIBA_N$) having significantly higher concentrations of those two VOCs than PIAL based on LME models (Table 2, Fig. 3B). Other influential whole plant VOCs and PVR compounds for PIAL *vs.*$PIBA_N$ and PIAL *vs.*$PIBA_S$ included α-pinene (Fig. 3C) and other compounds listed in Table 2. PIAL and $PIBA_S$ significantly differed in concentrations of total whole plant VOCs but not total PVR compounds, while PIAL and $PIBA_N$ did not differ in concentrations of either total whole plant VOCs or PVR (Figs. 4A, 5A). Consistently, whole plant VOCs more clearly separated between PIAL and $PIBA_S$ rather than $PIBA_N$ (Fig. 4B). In contrast to whole plant VOCs, PVR compounds clearly separated between PIAL and both $PIBA_S$ and $PIBA_N$ (Fig. 5B).

Drought vs. Control

We observed few significant trait differences between species in response to treatment (Table S3). Overall, across both species, the drought treatment had an 18% lower soil volumetric water content than the control treatment. Only four traits differed: drought A_S:A_L and guard cell area were higher than control for PIBA but not for PIAL, and drought LW ring width was greater and root starch concentration was lower than control for PIAL but not for PIBA. The most influential whole plant VOCs and PVR compounds driving the separation between treatments for both species are presented in Table S3. Of the influential whole plant VOCs, control had higher concentrations of unknown monoterpenes 3 and 4 than drought for PIBA but not for PIAL, while unknown sesquiterpene 5 or β-ocimene-2 did not differ between treatments for either species. We found no differences in any of the four influential PVR compounds for either species. Drought concentrations of total whole plant VOCs were lower than control for PIBA but not for PIAL while total PVR compound concentration did not differ between treatments for either species.

Discussion

PIAL and PIBA juveniles displayed different suites of traits that confer stress resistance to similar abiotic (high winds, drought, low temperatures) and biotic stressors (white pine blister rust, bark beetle). Though annual total precipitation of our PIAL juveniles' climate of origin was 20% lower than PIBA, PIAL did not always exhibit more drought stress-resistant traits than PIBA, contrary to hypothesis 1. In support of hypothesis 2, although $PIBA_N$ and $PIBA_S$ did not differ for most traits, $PIBA_S$ emitted higher concentrations of total whole plant VOCs and β-pinene (whole plant VOC), and had higher A_S:A_L and lower EW cell wall thickness than $PIBA_N$, possibly reflecting $PIBA_S$ originating from a drier and/or more herbivore- or pathogen-prone environment than $PIBA_N$. Contrary to hypothesis 3, traits of PIAL and $PIBA_S$ generally differed the most, while $PIBA_N$ was intermediate between PIAL and $PIBA_S$. We could not test hypothesis 4 because our drought treatment did not induce measurable physiological drought responses. Therefore, we have focused the Discussion on comparing traits of PIAL, $PIBA_N$, and $PIBA_S$.

PIAL and PIBA Displayed Different Suites of Traits to Confer Stress Resistance

Between the two species, juveniles of PIAL and PIBA displayed different traits that promote resistance to mechanical stress from high winds and to drought stress, common characteristics of their exposed, high-elevation habitats. This was supported by the observation that both our PIAL and PIBA juveniles' climates of origin experienced reduced precipitation but at different times of year with PIAL having drier winters and PIBA having drier summers. Low winter precipitation can result in growing season drought stress since high-elevation pines rely on snowmelt for

moisture throughout the summer (Moyes et al. 2013; Hankin and Bisbing 2021). Both species displayed different traits that increase stem and branch mechanical strength to withstand physical damage. Compared to PIBA, PIAL had shorter, thicker stems, higher stem diameter:stem height, and higher branch diameter:branch length than PIBA (Read and Stokes 2006), while PIBA had significantly smaller diameter and more densely packed LW (latewood) tracheids than PIAL (Domec and Gartner 2002). In addition to resisting mechanical stress, narrower, densely packed tracheids are more resistant to embolism and therefore increase PIBA hydraulic safety and drought resistance. Another consequence of narrower tracheids was a significantly lower K_p (potential hydraulic conductivity, total amount of water that can be transported through the stem) compared to PIAL, demonstrating the classic trade-off between hydraulic safety and hydraulic efficiency (McCulloh et al. 2019), commonly observed in drought-adapted species (Lachenbruch and McCulloh 2014; Fu et al. 2019). Wider tracheids increase the efficiency of water transport throughout the plant, which supports increased rates of photosynthesis, growth, and metabolism. However, wider tracheids are more vulnerable to embolism, which can result in hydraulic failure (Brodribb et al. 2017). PIAL displayed other traits conferring drought resistance. For example, compared to PIBA, PIAL exhibited higher LMA (leaf mass per area) and smaller stomatal (aperture) size, both of which reduce foliar water loss, increasing PIAL drought resistance (Reich et al. 1997; Wright et al. 2004). Higher LMA also may increase leaf life span to protect against cold stress (Takahashi and Miyajima 2008), consistent with the colder winter temperatures of PIAL than PIBA. Higher LMA also may increase light absorption (Poorter et al. 2009), which is consistent with PIAL having significantly higher canopy leaf area and lower STAR compared to PIBA.

We observed evidence for a lack of coordination between our measured xylem and stomatal traits, where PIBA exhibited significantly larger stomata, smaller LW lumen area, and higher LW tracheid density than PIAL. This was unexpected because xylem traits are often correlated with stomatal traits to support whole plant water transport where liquid water travels through xylem and gaseous water evaporates from stomata. For example, increased tracheid density and smaller tracheid size (lumen area) have been observed in tandem with higher stomatal density and smaller stomata (Brodribb et al. 2017; Zhong et al. 2020). Consistently, stomatal size has been shown to positively correlate with water availability, increasing hydraulic efficiency but reducing hydraulic safety (Guérin et al. 2018; Bertolino et al. 2019). Traits that were not measured in this study may compensate for this unexpected lack of coordination. For example, dynamic traits that describe stomatal kinetics (e.g., rate of stomatal opening and closing) may more strongly coordinate with xylem traits, as stomatal size and density are relatively static traits (Letts et al. 2009; Drake et al. 2013).

PIAL and PIBA appeared to have species-specific blends of VOC and PVR compounds where, compared to PIAL, PIBA exhibited significantly higher concentrations of 2 of the 4 most influential whole plant VOCs (including β-pinene) and of all 4 of the most influential PVR compounds (including α-pinene) (Table 2), and PVR compounds clearly separated between species (Fig. 5). This suggests that compared to PIAL, PIBA may be better equipped to resist stress because VOCs and PVR

compounds are secondary compounds that protect plants against abiotic and biotic stress (Bryant et al. 1983; Herms and Mattson 1992; Huang et al. 2019) including drought (Trowbridge et al. 2014, 2021) and mountain pine beetles (Gray et al. 2015; Eidson et al. 2018). However, such secondary compounds can also increase susceptibility to biotic stress because bark beetles are attracted to α-pinene and use it to produce aggregating pheromones (Hughes 1974; Byers and Birgersson 1990). VOCs and PVR compounds are created in a process that requires the metabolism of NSC (Kozlowski 1992). PIBA had significantly higher concentrations of needle and stem soluble sugars (glucose, fructose, sucrose) than PIAL, which may contribute to higher PIBA whole plant VOC β-pinene and PVR α-pinene concentrations than PIAL. Higher sugar concentrations also may increase PIBA drought resistance because low-molecular weight soluble sugars can be transported rapidly for functions such as osmoregulation to maintain turgor and function (Hartmann and Trumbore 2016).

To our knowledge, this is the first study to compare and measure whole plant VOC and PVR compounds in PIBA and PIAL juveniles. A previous study measured VOCs in mature trees in the field, which detected no difference in total VOC emissions between PIBA and PIAL (Runyon et al. 2020), matching our finding that VOC emissions did not significantly differ between juveniles of these species. Additionally, the blend of VOCs emitted by juveniles in our study is consistent with that emitted by mature trees of both species (Runyon et al. 2020), suggesting that some juvenile defense mechanisms may be related to adult defense mechanisms. However, PVR studies of mature PIBA VOCs have found much higher concentrations than we found in juveniles (Bentz et al. 2017; Runyon et al. 2022), highlighting that adults and juveniles may respond to or be affected by stress in different ways. For example, mountain pine beetles only attack larger mature trees (Bentz et al. 2017, 2022), which could explain why mature individuals have higher constitutive terpene concentrations. We found PIBA had higher resin duct density and area than PIAL, both of which may increase resistance against bark beetles (Hood et al. 2020) because resin ducts are permanently embedded into the stem. Resin is synthesized and stored within resin ducts in coniferous species and functions as both a physical and chemical defense mechanism (Vázquez-González et al. 2020). Larger resin ducts have correlated with higher concentrations of certain PVR compounds while increased resin duct density had variable effects depending on the compound (Mason et al. 2019). Notably, we measured constitutive VOCs in this study, while defense to biotic agents also can be induced upon attack (Kutty and Mishra 2023).

PIBAS Had Higher VOC Concentrations than PIBAN

Compared to $PIBA_N$, $PIBA_S$ emitted higher concentrations of four whole plant VOCs (β-pinene, unknown benzene 1, unknown monoterpene 4, total VOCs) and one PVR compound (methyl thymyl ether), which may reflect the drier climate of origin of $PIBA_S$ and/or that the previous exposure and/or susceptibility to herbivores or pathogens of $PIBA_S$ may differ from $PIBA_N$. Water stress has been linked to higher emissions of VOCs (Holopainen and Gershenzon 2010), which may be a

result of functional traits or higher vapor pressure promoting VOC emissions. To our knowledge, PIBA population differences in susceptibility to biotic or abiotic stress have not been tested. We observed only two non-VOC traits that differed between populations, and both also supported hypothesis 2. $PIBA_S$ had significantly higher A_S:A_L than $PIBA_N$, suggesting that $PIBA_S$ may be more drought resistant because higher A_S:A_L reduces the leaf area through which water can be lost through transpiration (Togashi et al. 2015). $PIBA_N$ had significantly higher EW cell wall thickness than $PIBA_S$, which can increase hydraulic efficiency and water transport, which is more likely to occur in the wetter $PIBA_N$ climate of origin than $PIBA_S$.

Traits of PIAL were more Similar to PIBAN than PIBAS

We observed a gradient in trait values from PIAL to $PIBA_N$ to $PIBA_S$ (and vice versa) for the majority of our measured traits (whole plant VOCs NMDS, total VOC concentration, β-pinene (VOC), α-pinene (PVR), and 9 morphological and physiological traits). This result may suggest that growing season precipitation may have influenced the gradient in traits from PIAL to $PIBA_N$ to $PIBA_S$ more strongly than winter and annual precipitation. Annual total precipitation of our juveniles' climates of origin was highest in $PIBA_N$, followed by PIAL, and then $PIBA_S$, growing season total precipitation was highest in PIAL, then $PIBA_N$, and then $PIBA_S$, while winter season total precipitation was highest in $PIBA_N$, then $PIBA_S$, and then PIAL. This was unexpected because we had hypothesized that PIAL and $PIBA_S$ would be most similar based on the expectation that the annual total precipitation of PIBA (mean of both populations) would be higher than that of PIAL, and annual total precipitation of $PIBA_N$ would be higher than that of $PIBA_S$. Importantly, our study compared PIAL from the Rocky Mountains with PIBA from California, despite that PIAL exists in California as well. Given this, we cannot disentangle the effect of species and climate (location) of origin on observed trait differences between PIAL and PIBA because PIAL and PIBA in this study originated from different locations.

Drought Treatment did not Induce Physiological Response

Although the drought treatment resulted in 18% lower VWC than the control treatment, pre-dawn and midday leaf water potentials, g_s (stomatal conductance), A_{net} (photosynthesis), and health status did not differ between treatments, and only four traits differed between treatments, suggesting that the drought treatment did not induce a biologically meaningful physiological response in our study trees. The minimal effect of our drought treatment most likely occurred due to the Marchin et al. (2020) method we had selected to simulate long-term drought progression in the field. This method was originally developed on tropical plant species which are faster-growing and adapted to utilizing surface water (Marchin et al. 2022). In contrast, PIBA and PIAL are slow-growing species that use water more slowly and have deeper root systems to access water deep in the soil when precipitation is scarce (Campbell et al. 2011).

Conclusions

Our study improves our understanding of the physiological mechanisms that may underlie PIAL and PIBA current and future distributions. We observed that PIAL and PIBA displayed different suites of traits that enable them to resist similar stressors including high winds and drought, and persist in their high-elevation habitats. $PIBA_N$ and $PIBA_S$ most notably differed in VOC emissions, with $PIBA_S$ emitting higher whole plant VOC concentrations, suggesting that the disjunct PIBA populations may differ in their susceptibility to stress. For most of our measured traits, PIAL and $PIBA_N$ were most similar while PIAL and $PIBA_S$ differed the most, reflecting the same pattern in growing season total precipitation of each group. Together, our results suggest that changes in environmental stress may affect PIAL, $PIBA_S$, and $PIBA_N$ in different ways and further investigation is needed to better understand their responses to future global change.

Supplementary Information The online version contains supplementary material available at https://doi.org/10.1007/s44391-025-00040-w.

Acknowledgements Thanks to the USDA Forest Service Dorena Genetics Lab and Coeur d'Alene Nursery for donating plant material, Ian Laga for help with multivariate statistics and experimental design, and Maria Jerome for help with xylem image processing. Thanks to Jessica Harris, Teodora Rautu, Lou Duloisy, Stephen Huysman, Chloe Wasteneys, Ethan Fuchs, Bobby Beers, Tristan Burlingame, Timothy Jones, Grace Miller, Naomi Vliet, Benjamin Spiers, William Lutz, Gabrielle Ostrowski, David Heinson, and David Rossal for assistance. This research was supported in part by the USDA Forest Service, Rocky Mountain Research Station. The findings and conclusions in this publication are those of the authors and should not be construed to represent any official USDA or US. Government determination or policy

Author Contributions Conceptualization and Methodology – KS, DU, KB; Data Collection—KS, SH-S, FA, JR; Data Analysis—KS, DU, JR, BS; Original Manuscript Draft Preparation—KS and DU; Manuscript Review & Editing—KS, DU, JR, KB, BS, SH-S, FA; and Funding Acquisition – DU, KS. All authors read and approved the final manuscript.

Funding This research was supported by Montana State University, the USDA Forest Service Forest Health Protection program, and the Whitebark Pine Ecosystem Foundation student research grant.

Data Availability All data can be made available upon reasonable request to the corresponding author.

Declarations

Competing interests The authors declare no competing interests.

References

Baumeister, D., and R. M. Callaway. 2006. Facilitation by pinus flexilis during succession: a hierarchy of mechanisms benefits other plant species. *Ecology* 87:1816–1830. https://doi.org/10.1890/0012-9658(2006)87[1816:FBPFDS]2.0.CO;2.

Bentz, B. J., S. M. Hood, E. M. Hansen, J. C. Vandygriff, and K. E. Mock. 2017. Defense traits in the long-lived Great Basin bristlecone pine and resistance to the native herbivore mountain pine beetle. *New Phytologist* 213(2): 611–624.

Bentz, B. J., E. M. Hansen, M. Davenport, D. Soderberg. 2022. Complexities in predicting mountain pine beetle and spruce beetle response to climate change. In: *Bark Beetle Management, Ecology, and Climate Change*. Elsevier, pp 31–54.

Bertolino, L. T., R. S. Caine, and J. E. Gray. 2019. Impact of stomatal density and morphology on water-use efficiency in a changing world. *Frontiers in Plant Science* 10:225. https://doi.org/10.3389/fpls.2019.00225.

Brodribb, T. J., S. A. McAdam, and M. R. Carins Murphy. 2017. Xylem and stomata, coordinated through time and space. *Plant, Cell & Environment* 40:872–880. https://doi.org/10.1111/pce.12817.

Bryant, J. P., F. S. Chapin, and D. R. Klein. 1983. Carbon/nutrient balance of boreal plants in relation to vertebrate herbivory. *Oikos* 40:357–368. https://doi.org/10.2307/3544308.

Bunn, A. G., M. W. Salzer, K. J. Anchukaitis, et al. 2018. Spatiotemporal variability in the climate growth response of high elevation bristlecone pine in the white mountains of California. *Geophysical Research Letters* 45:13,312-13,321. https://doi.org/10.1029/2018GL080981.

Burkle, L., and J. Runyon. 2017. The smell of environmental change: using floral scent to explain shifts in pollinator attraction. *Applications in Plant Sciences* 5:1600123. https://doi.org/10.3732/apps.1600123.

Byers, J. A., and G. Birgersson. 1990. Pheromone production in a bark beetle independent of myrcene precursor in host pine species. *Naturwissenschaften* 77:385–387. https://doi.org/10.1007/BF01135739.

Campbell, E. M., R. E. Keane, E. R. Larson, M. P. Murray, A. W. Schoettle, and C. Wong. 2011. Disturbance ecology of high_elevation five-needle pine ecosystems in western North America. In *The future of high-elevation, five-needle white pines in Western North America: Proceedings of the High Five Symposium. 28-30 June 2010; Missoula, MT. Proceedings RMRS-P-63*, ed. Robert E. Keane, Diana F. Tomback, Michael P. Murray, and Cyndi M. Smith, vol. 63, 154–163. Fort Collins, CO: US Department of Agriculture, Forest Service, Rocky Mountain Research Station.

Chang, T., A. J. Hansen, and N. Piekielek. 2014. Patterns and variability of projected bioclimatic habitat for pinus albicaulis in the greater yellowstone area. *PLoS ONE* 9:e111669. https://doi.org/10.1371/journal.pone.0111669.

Domec, J., and B. L. Gartner. 2002. How do water transport and water storage differ in coniferous earlywood and latewood? *Journal of Experimental Botany* 53:2369–2379. https://doi.org/10.1093/jxb/erf100.

Drake, P. L., R. H. Froend, and P. J. Franks. 2013. Smaller, faster stomata: scaling of stomatal size, rate of response, and stomatal conductance. *Journal of Experimental Botany* 64:495–505. https://doi.org/10.1093/jxb/ers347.

Dullinger, S., T. Dirnböck, and G. Grabherr. 2004. Modelling climate change-driven treeline shifts: relative effects of temperature increase, dispersal and invasibility. *Journal of Ecology* 92:241–252. https://doi.org/10.1111/j.0022-0477.2004.00872.x.

Duriscoe, D. M., and C. S. Duriscoe. 2002. *Survey and monitoring of white pine blister rust in Sequoia and Kings Canyon NationalParks: Final report on 1995–1999 survey and monitoring plot network*, 34 p. Science and Natural Resources Management Division, Sequoia and Kings Canyon National Parks, Three Rivers, CA: Tech. Rep.

Eckert, A. J., B. R. Tearse, and B. D. Hall. 2008. A phylogeographical analysis of the range disjunction for foxtail pine (Pinus balfouriana, Pinaceae): the role of Pleistocene glaciation. *Molecular Ecology* 17 (18): 3852–3865.

Eidson, E. L., K. E. Mock, and B. J. Bentz. 2018. Low offspring survival in mountain pine beetle infesting the resistant great basin bristlecone pine supports the preference-performance hypothesis. *PLoS ONE* 13:e0196732. https://doi.org/10.1371/journal.pone.0196732.

Government of Canada. (2017). Recovery strategy for the whitebark pine (Pinus albicaulis) in Canada.

Farnes, P. E. 1990. SNOTEL and snow course data: describing the hydrology of whitebark pine ecosystems, 302–304. In *Proc. Symp. on Whitebark Pine Ecosystems: Ecology and Management of a High-Mountain Resource, Gen. Tech. Rep. INT-270*. Ogden, UT: USDA Forest Service, Intermountain Research Station.

Felicetti, L. A., C. C. Schwartz, R. O. Rye, et al. 2003. Use of sulfur and nitrogen stable isotopes to determine the importance of whitebark pine nuts to Yellowstone grizzly bears. *Canadian Journal of Zoology* 81:763–770. https://doi.org/10.1139/z03-054.

Fiedler, C. E., and S. T. McKinney. 2014. Forest structure, health, and mortality in two rocky mountain whitebark pine ecosystems: implications for restoration. *Natural Areas Journal* 34:290–299. https://doi.org/10.3375/043.034.0305.

Fryer, Janet L. 2004. Pinus balfouriana. In: Fire Effects Information System, [Online]. USDA Forest Service, Rocky Mountain Research Station, Fire Sciences Laboratory. www.fs.usda.gov/database/feis/plants/tree/pinbal/all.html. Accessed 19 Nov 2023.

Fu, X., F. C. Meinzer, D. R. Woodruff, et al. 2019. Coordination and trade-offs between leaf and stem hydraulic traits and stomatal regulation along a spectrum of isohydry to anisohydry. *Plant, Cell & Environment* 42:2245–2258. https://doi.org/10.1111/pce.13543.

Gibson, K., K. Skov, S. Kegley, J. Jorgensen, S. Smith, and J. Witcosky. 2008. *Mountain pine beetle impacts in high-elevation five_needle pines: current trends and challenges. FHTET-2008-2*, 32 p. Fort Collins, CO: USDA Forest Service, Forest Health Protection, Forest Health Technology Enterprise Team.

Goeking, S. A., and M. A. Windmuller-Campione. 2021. Comparative species assessments of five-needle pines throughout the western United States. *Forest Ecology and Management* 496:119438. https://doi.org/10.1016/j.foreco.2021.119438.

Gray, C. A., J. B. Runyon, M. J. Jenkins, and A. D. Giunta. 2015. Mountain pine beetles use volatile cues to locate host limber pine and avoid non-host great basin bristlecone pine. *PLoS ONE* 10:e0135752. https://doi.org/10.1371/journal.pone.0135752.

Guérin, M., D. Martin-Benito, G. Arx, et al. 2018. Interannual variations in needle and sapwood traits of *Pinus edulis* branches under an experimental drought. *Ecology and Evolution* 8:1655–1672. https://doi.org/10.1002/ece3.3743.

Hacke, U. G., J. S. Sperry, W. T. Pockman, et al. 2001. Trends in wood density and structure are linked to prevention of xylem implosion by negative pressure. *Oecologia* 126:457–461. https://doi.org/10.1007/s004420100628.

Hankin, L. E., and S. M. Bisbing. 2021. Let it snow? Spring snowpack and microsite characterize the regeneration niche of high-elevation pines. *Journal of Biogeography* 48:2068–2084. https://doi.org/10.1111/jbi.14136.

Hansen, A., K. Ireland, K. Legg, et al. 2016. Complex challenges of maintaining whitebark pine in greater yellowstone under climate change: a call for innovative research, management, and policy approaches. *Forests* 7:54. https://doi.org/10.3390/f7030054.

Hansen, A. J., A. East, R. E. Keane, et al. 2021. Is whitebark pine less sensitive to climate warming when climate tolerances of juveniles are considered? *Forest Ecology and Management* 493:19221. https://doi.org/10.1016/j.foreco.2021.119221.

Hartmann, H., and S. Trumbore. 2016. Understanding the roles of nonstructural carbohydrates in forest trees – from what we can measure to what we want to know. *New Phytologist* 211:386–403. https://doi.org/10.1111/nph.13955.

Herms, D. A., and W. J. Mattson. 1992. The dilemma of plants: to grow or defend. *The Quarterly Review of Biology* 67:283–335. https://doi.org/10.1086/417659.

Holopainen, J. K., and J. Gershenzon. 2010. Multiple stress factors and the emission of plant VOCs. *Trends in Plant Science* 15:176–184. https://doi.org/10.1016/j.tplants.2010.01.006.

Hood, S. M., C. C. Reed, and J. M. Kane. 2020. Axial resin duct quantification in tree rings: a functional defense trait. *MethodsX* 7:101035. https://doi.org/10.1016/j.mex.2020.101035.

Huang, J., A. Hammerbacher, A. Weinhold, et al. 2019. Eyes on the future – evidence for trade-offs between growth, storage and defense in Norway spruce. *New Phytologist* 222:144–158. https://doi.org/10.1111/nph.15522.

Hughes, P. R. 1974. Myrcene: a precursor of pheromones in Ips beetles. *Journal of Insect Physiology* 20:1271–1275. https://doi.org/10.1016/0022-1910(74)90232-7.

IUCN. 2024. *The IUCN Red List of Threatened Species*. International Union for Conservation of Nature. Available online at https://iucn.org/resources/conservation-tool/iucn-red-list-threatened-species.

Keane, R. E., L. M. Holsinger, M. F. Mahalovich, and D. F. Tomback. 2017. *Restoring whitebark pine ecosystems in the face of climate change*. Gen. Tech. Rep. RMRS-GTR-361, 123. Fort Collins, CO: USDA Forest Service, Rocky Mountain Research Station.

Kozlowski, T. 1992. Carbohydrate sources and sinks in woody plants. *The Botanical Review* 58:107–222.

Kutty, N. N., and M. Mishra. 2023. Dynamic distress calls: Volatile info chemicals induce and regulate defense responses during herbivory. *Frontiers in Plant Science* 14:1135000.

Lachenbruch, B., and K. A. McCulloh. 2014. Traits, properties, and performance: how woody plants combine hydraulic and mechanical functions in a cell, tissue, or whole plant. *New Phytologist* 204:747–764. https://doi.org/10.1111/nph.13035.

Landguth, E. L., Z. A. Holden, M. F. Mahalovich, and S. A. Cushman. 2017. Using landscape genetics simulations for planting blister rust resistant whitebark pine in the US Northern Rocky Mountains. *Frontiers in Genetics*. 8:9.

Landhäusser, S. M., P. S. Chow, L. T. Dickman, et al. 2018. Standardized protocols and procedures can precisely and accurately quantify non-structural carbohydrates. *Tree Physiology* 38:1764–1778. https://doi.org/10.1093/treephys/tpy118.

Letts, M. G., K. N. Nakonechny, K. E. Van Gaalen, and C. M. Smith. 2009. Physiological acclimation of Pinus flexilis to drought stress on contrasting slope aspects in Waterton Lakes National Park, Alberta, Canada. *Canadian Journal of Forest Research* 39:629–641. https://doi.org/10.1139/X08-206.

Marchin, R. M., A. Ossola, M. R. Leishman., D. S. Ellsworth. 2020. A simple method for simulating drought effects on plants. *Front Plant Sci* 10. https://doi.org/10.3389/fpls.2019.01715.

Marchin, R. M., D. Backes, A. Ossola, et al. 2022. Extreme heat increases stomatal conductance and drought-induced mortality risk in vulnerable plant species. *Global Change Biology* 28:1133–1146. https://doi.org/10.1111/gcb.15976.

Martínez-Berdeja, A., J. A. Hamilton, A. Bontemps, et al. 2019. Evidence for population differentiation among Jeffrey and Ponderosa pines in survival, growth and phenology. *Forest Ecology and Management* 434:40–48. https://doi.org/10.1016/j.foreco.2018.12.009.

Mason, C. J., K. Keefover-Ring, C. Villari, et al. 2019. Anatomical defences against bark beetles relate to degree of historical exposure between species and are allocated independently of chemical defences within trees. *Plant, Cell & Environment* 42:633–646. https://doi.org/10.1111/pce.13449.

McCulloh, K. A., J.-C. Domec, D. M. Johnson, et al. 2019. A dynamic yet vulnerable pipeline: Integration and coordination of hydraulic traits across whole plants. *Plant, Cell & Environment* 42:2789–2807. https://doi.org/10.1111/pce.13607.

Moore, P. E., O. Alvarez, S. T. McKinney, W. Li, M. L. Brooks, and Q. Guo. 2017. *Climate change and tree-line ecosystems in the Sierra Nevada: Habitat suitability modelling to inform high-elevation forest dynamics monitoring*. U.S. Geological Survey Report 19. PRISM Group, Oregon State University. https://prism.oregonstate.edu. Accessed 11 Sep 2023.

Moyes, A. B., C. Castanha, M. J. Germino, and L. M. Kueppers. 2013. Warming and the dependence of limber pine (Pinus flexilis) establishment on summer soil moisture within and above its current elevation range. *Oecologia* 171:271–282. https://doi.org/10.1007/s00442-012-2410-0.

Nesmith, J. C. B., M. Wright, E. S. Jules, and S. T. McKinney. 2019. Whitebark and foxtail pine in Yosemite, sequoia, and kings canyon national parks: initial assessment of stand structure and condition. *Forests* 10:35. https://doi.org/10.3390/f10010035.

Oline, D. K., J. B. Mitton, and M. C. Grant. 2000. Population and subspecific genetic differentiation in the foxtail pine (Pinus balfouriana). *Evolution* 54:1813–1819. https://doi.org/10.1111/j.0014-3820.2000.tb00725.x.

Pepin, N., R. S. Bradley, H. F. Diaz, et al. 2015. Elevation-dependent warming in mountain regions of the world. *Nature Climate Change* 5:424–430. https://doi.org/10.1038/nclimate2563.

Poorter, H., Ü. Niinemets, L. Poorter, et al. 2009. Causes and consequences of variation in leaf mass per area (LMA): A meta-analysis. *New Phytologist* 182:565–588. https://doi.org/10.1111/j.1469-8137.2009.02830.x.

PRISM Climate Group at Oregon State University. n.d. https://prism.oregonstate.edu/normals/. Accessed 11 Sep 2023.

Read, J., and A. Stokes. 2006. Plant biomechanics in an ecological context. *American Journal of Botany* 93:1546–1565. https://doi.org/10.3732/ajb.93.10.1546.

Reich, P. B., M. B. Walters, and D. S. Ellsworth. 1997. From tropics to tundra: global convergence in plant functioning. *Proc Natl Acad Sci U S A* 94:13730–13734.

Reutemann, P. 2022. Fastrandomforest-weka-package.

Rissanen, K., J. Aalto, A. Gessler, et al. 2022. Drought effects on volatile organic compound emissions from Scots pine stems. *Plant, Cell & Environment* 45:23–40. https://doi.org/10.1111/pce.14219.

Runyon, J. B., C. A. Gray, and M. J. Jenkins. 2020. Volatiles of high-elevation five-needle pines: chemical signatures through ratios and insight into insect and pathogen resistance. *Journal of Chemical Ecology* 46:264–274. https://doi.org/10.1007/s10886-020-01150-0.

Runyon, J. B., B. J. Bentz, and C. A. Qubain. 2022. Constitutive and induced defenses in long-lived pines do not trade off but are influenced by climate. *Journal of Chemical Ecology* 48:746–760. https://doi.org/10.1007/s10886-022-01377-z.

Schaming, T. D., and C. S. Sutherland. 2020. Landscape- and local-scale habitat influences on occurrence and detection probability of Clark's nutcrackers: Implications for conservation. *PLoS ONE* 15:e0233726. https://doi.org/10.1371/journal.pone.0233726.

Schindelin, J., I. Arganda-Carreras, E. Frise, et al. 2012. Fiji: an open-source platform for biological-image analysis. *Nature Methods* 9:676–682. https://doi.org/10.1038/nmeth.2019.

Schoettle, A. W., K. S. Burns, S. T. McKinney, et al. 2022. Integrating forest health conditions and species adaptive capacities to infer future trajectories of the high elevation five-needle white pines. *Forest Ecology and Management* 521:120389. https://doi.org/10.1016/j.foreco.2022.120389.

Sniezko, R. A., and J.-J. Liu. 2022. Genetic resistance to white pine blister rust, restoration options, and potential use of biotechnology. *Forest Ecology and Management* 520:120168. https://doi.org/10.1016/j.foreco.2022.120168.

Steppe, K., and R. Lemeur. 2007. Effects of ring-porous and diffuse-porous stem wood anatomy on the hydraulic parameters used in a water flow and storage model. *Tree Physiology* 27:43–52. https://doi.org/10.1093/treephys/27.1.43.

Sterck, F. J., R. Zweifel, U. Sass-Klaassen, and Q. Chowdhury. 2008. Persisting soil drought reduces leaf specific conductivity in scots pine (Pinus sylvestris) and pubescent oak (Quercus pubescens). *Tree Physiology* 28:529–536. https://doi.org/10.1093/treephys/28.4.529.

Takahashi, K., and Y. Miyajima. 2008. Relationships between leaf life span, leaf mass per area, and leaf nitrogen cause different altitudinal changes in leaf δ13C between deciduous and evergreen species. *Botany* 86:1233–1241. https://doi.org/10.1139/B08-093.

Thoma, D. P., E. K. Shanahan, and K. M. Irvine. 2019. Climatic correlates of white pine blister rust infection in whitebark pine in the greater yellowstone ecosystem. *Forests* 10:666. https://doi.org/10.3390/f10080666.

Togashi, H. F., I. C. Prentice, B. J. Evans, et al. 2015. Morphological and moisture availability controls of the leaf area-to-sapwood area ratio: Analysis of measurements on Australian trees. *Ecology and Evolution* 5:1263–1270. https://doi.org/10.1002/ece3.1344.

Tomback, D. F., A. J. Anderies, K. S. Carsey, et al. 2001. Delayed seed germination in whitebark pine and regeneration patterns following the yellowstone fires. *Ecology* 82:2587–2600. https://doi.org/10.1890/0012-9658(2001)082[2587:DSGIWP]2.0.CO;2.

Tomback, D. F., R. E. Keane, A. W. Schoettle, et al. 2022. Tamm review: current and recommended management practices for the restoration of whitebark pine (Pinus albicaulis Engelm.), an imperiled high-elevation Western North American forest tree. *Forest Ecology and Management* 522:119929. https://doi.org/10.1016/j.foreco.2021.119929.

Tran, T. J., J. M. Bruening, A. G. Bunn, et al. 2017. Cluster analysis and topoclimate modeling to examine bristlecone pine tree-ring growth signals in the Great Basin, USA. *Environmental Research Letters* 12:014007. https://doi.org/10.1088/1748-9326/aa5388.

Trowbridge, A. M., R. W. Daly, D. Helmig, et al. 2014. Herbivory and climate interact serially to control monoterpene emissions from pinyon pine forests. *Ecology* 95:1591–1603. https://doi.org/10.1890/13-0989.1.

Trowbridge, A. M., H. D. Adams, A. Collins, et al. 2021. Hotter droughts alter resource allocation to chemical defenses in piñon pine. *Oecologia* 197:921–938. https://doi.org/10.1007/s00442-021-05058-8.

Ulrich, D. E. M., C. Wasteneys, S. Hoy-Skubik, and F. Alongi. 2023. Functional traits underlie specialist-generalist strategies in whitebark pine and limber pine. *Forest Ecology and Management* 542:121113. https://doi.org/10.1016/j.foreco.2023.121113.

USFWS. 2022. Endangered and threatened wildlife and plants; threatened species status with section 4(d) rule for whitebark pine (Pinus albicaulis). In: federal register. https://www.federalregister.gov/documents/2022/12/15/2022-27087/endangered-and-threatened-wildlife-and-plants-threatened-species-status-with-section-4d-rule-for. Accessed 19 Nov 2023.

Vázquez-González, C., R. Zas, N. Erbilgin, et al. 2020. Resin ducts as resistance traits in conifers: linking dendrochronology and resin-based defences. *Tree Physiology* 40:1313–1326. https://doi.org/10.1093/treephys/tpaa064.

Wright, I. J., P. B. Reich, M. Westoby, et al. 2004. The worldwide leaf economics spectrum. *Nature* 428:821–827. https://doi.org/10.1038/nature02403.

Wyka, S. A., I. A. Munck, N. J. Brazee, and K. D. Broders. 2018. Response of eastern white pine and associated foliar, blister rust, canker and root rot pathogens to climate change. *Forest Ecology and Management* 423:18–26. https://doi.org/10.1016/j.foreco.2018.03.011.

Yang, S., F. J. Sterck, U. Sass-Klaassen, et al. 2022. Stem trait spectra underpin multiple functions of temperate tree species. *Frontiers in Plant Science* 13:769551. https://doi.org/10.3389/fpls.2022.769551.

Young, D. J. N., M. R. Slaton, and A. Koltunov. 2023. Temperature is positively associated with tree mortality in California subalpine forests containing whitebark pine. *Ecosphere* 14:e4400. https://doi.org/10.1002/ecs2.4400.

Zhong, M., B. E. L. Cerabolini, P. Castro-Díez, et al. 2020. Allometric co-variation of xylem and stomata across diverse woody seedlings. *Plant, Cell and Environment* 43:2301–2310. https://doi.org/10.1111/pce.13826.

Authors and Affiliations

Katherine Sparks[1] · Sean L. Hoy-Skubik[2] · Franklin Alongi[3] · Justin B. Runyon[4] · Katharine M. Banner[5] · Brian V. Smithers[2] · Danielle E. M. Ulrich[2]

✉ Danielle E. M. Ulrich
Danielle.Ulrich@montana.edu

1 USDA Forest Service Placerville Nursery, Camino, CA, USA

2 Department of Ecology, Montana State University, Bozeman, MT, USA

3 Karlsruhe Institute of Technology (KIT), Institute of Meteorology and Climate Research - Atmospheric Environmental Research (IMK-IFU), 82467 Garmisch-Partenkirchen, Germany

4 USDA Forest Service Rocky Mountain Research Station, Bozeman, MT, USA

5 Department of Mathematical Sciences, Montana State University, Bozeman, MT, USA